J Biomol NMR (2015) 63:315–321
DOI 10.1007/s10858-015-9988-6

NMR STRUCTURE NOTE

The C-terminal domain of human Cdc37 studied by solution NMR

Ziming Zhang[1] · Dimitra Keramisanou[1] · Amit Dudhat[1] · Michael Paré[1] · Ioannis Gelis[1]

Received: 7 August 2015 / Accepted: 19 September 2015 / Published online: 24 September 2015

Biological context

Cancer cells are characterized by misregulated protein homeostasis and accumulation of overexpressed, mutated or otherwise unstable oncogenic proteins. To cope with these stress conditions, cancer cells harness the protective properties of protein chaperones. Among them, Hsp90 is unique in that its clients are implicated in all hallmark steps of the malignant transformation (Calderwood et al. 2006; Whitesell and Lindquist 2005). Cdc37 is the kinome-specific cochaperone of Hsp90 (Caplan et al. 2007; Karnitz and Felts 2007; Pearl 2005). Although in yeast it displays independent chaperone activity, in higher eukaryotes it is considered a gain-of-specificity cochaperone required to recruit protein kinases and facilitate their association with Hsp90 (Pearl and Prodromou 2006). In addition, it is considered an important mediator of cancer initiation and progression (Schwarze et al. 2003; Stepanova et al. 2000a, b) and thus it offers a very attractive alternative to Hsp90 inhibition, which shows mechanistic (activation of heat shock response) and clinical (toxicity) limitations (Bagatell et al. 2000; Jhaveri et al. 2012; McCollum et al. 2006; Sreeramulu et al. 2009a).

For protein kinases, the Hsp90-mediated chaperone cycle occurs at a late stage of folding to elicit fine structural changes to the kinase catalytic core that promote downstream functions or bring thermodynamic stability (Caplan et al. 2007). The cycle begins with kinase recognition by Cdc37. Transfer of the substrate to Hsp90 is facilitated by the ability of the cochaperone to arrest Hsp90's ATPase activity. Cdc37 release, remodeling of the kinase and its subsequent release from Hsp90 are all steps mediated by conformational changes that occur to Hsp90 (Pearl and Prodromou 2006). Progression through the cycle is finely modulated by phosphorylation and dephosphorylation of both Cdc37 and Hsp90, the presence of other co-chaperones and the identity of the nucleotide bound to Hsp90 (Rohl et al. 2013).

At a molecular level, the function of Cdc37 has been characterized at high resolution only with respect to its interaction with Hsp90 and the mechanism of the ATPase inhibition. Docking of the middle-domain of Cdc37 (Fig. 1a, M-Cdc37) at the ATP binding domain of Hsp90 positions $R167^{Cdc37}$ into the ATP pocket, which forms a hydrogen bond with the catalytic $E47^{Hsp90}$, resulting in the displacement of the bound nucleophilic water (Roe et al. 1999; Sreeramulu et al. 2009b). On the other hand, the recognition of protein kinases by the cochaperone and the transfer to Hsp90 are poorly understood steps of the cycle (Vaughan et al. 2006). Several residues at the N-terminus of Cdc37 have been identified as critical for the chaperoning of protein kinases (Polier et al. 2013; Shao et al. 2003a, b; Xu et al. 2012); however the structure of the putative substrate binding domain is still not known (Fig. 1a, N-Cdc37). In higher eukaryotes, the C-terminal domain (Fig. 1a, C-Cdc37) has also been implicated in kinase processing. Mutation of the invariant W342 to a cysteine impairs signaling by the sevenless receptor tyrosine kinase and causes a lethal defect at the pupal stage of Drosophila (Cutforth and Rubin 1994). In addition, phosphorylation of Y298 by YES has a detrimental effect on the interaction of Cdc37 with a diverse set of client kinases

Electronic supplementary material The online version of this article (doi:10.1007/s10858-015-9988-6) contains supplementary material, which is available to authorized users.

✉ Ioannis Gelis
igelis@usf.edu

[1] Department of Chemistry, University of South Florida, 4202 E. Fowler Ave. CHE 205, Tampa, FL 33620, USA

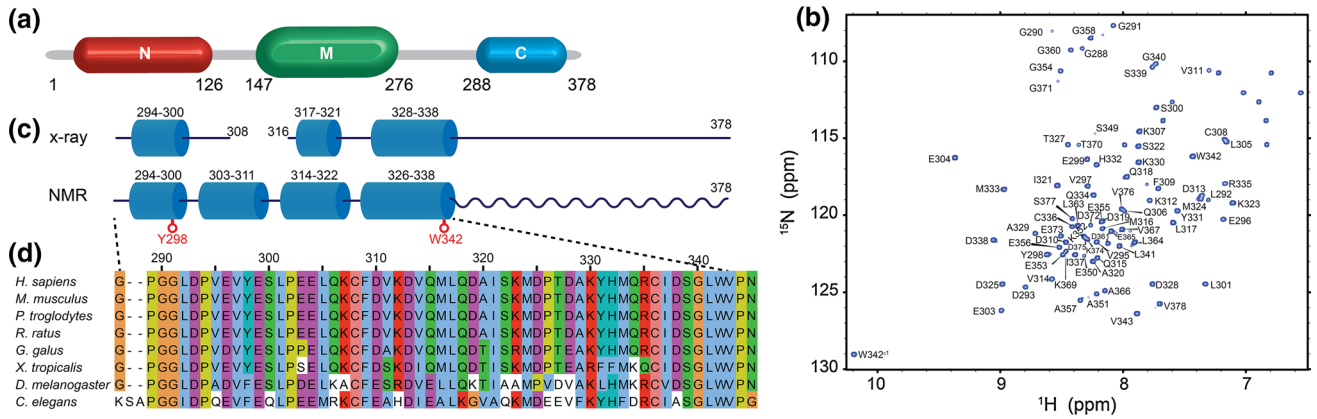

Fig. 1 **a** Schematic diagram of domain organization of Cdc37 based on published structural (PDB IDs: 1US7) (Roe et al. 2004; Sreeramulu et al. 2009b) and biochemical information. Residue numbering for domain boundaries refer to human Cdc37. **b** Fingerprint ^{1}H–^{15}N HSQC spectrum of C-Cdc37 (0.4 mM), acquired at 800 MHz and 30 °C showing the assignment. No signal is observed for a stretch of 5 residues (P344-A348). **c** Boundaries of secondary structure elements identified from the available crystal structure (*top*) and predicted from NMR chemical shifts using *TALOS-N* (*bottom*). The position of Y298 and W342 that are implicated in kinase processing are highlighted in red. **d** Multiple sequence alignment of the first 58 residues of the C-terminal domain of Cdc37 showing the high degree of conservation for this region

(Xu et al. 2012). The structure of C-Cdc37 was determined by X-ray crystallography in the context of a two-domain fragment encompassing also the middle domain (MC-Cdc37) in complex with the N-terminal domain of Hsp90 (Supplementary Fig. 1) (Roe et al. 2004). The structure revealed that C-Cdc37 has an overall helical topology, but it suffers from very high B-factors (average is 64.3) and no interpretable electron density for the segments 309–315 and 348–378.

As a first step toward a detailed mechanistic understanding of the role of C-Cdc37 in kinase chaperoning we have characterized its conformational properties using NMR. In solution, the core of C-Cdc37 folds into a small V-shaped bundle of four helices with an exposed patch of highly conserved hydrophobic residues. Compared to the crystal structure, a distinct helical registry is identified for one helix and an unresolved helix is refined. Mobility studies indicate that the C-terminal end of the domain forms a highly flexible tail, while part of the crystallographically unresolved regions undergo significant conformational fluctuations at a μs–ms timescale.

Methods

Cloning, expression, and purification of C-Cdc37

The N-terminal boundary for C-Cdc37 (residues G288-V378) was selected on the basis of the available crystal structure (Roe et al. 1999), where M- and C-Cdc37 are connected through an unstructured glycine/proline region (Supplementary Fig. 1). C-Cdc37 was PCR amplified with flanking BamHI and NdeI restriction sites and a stop codon was included. The PCR product was cloned into a pDB.His.MBP vector (Seiler et al. 2014) which carries a His_6-MBP N-terminal purification tag followed by a TEV cleavage site. The construct was transformed into BL21(DE3) and selected by kanamycin. Cells were cultured in M9 minimal media supplemented with $^{15}NH_4Cl$ and U-^{13}C6 glucose, trace metals and 2 % bioexpress (CIL), and incubated at 37 °C until $OD_{600} \sim 0.5$. Protein expression was induced by the addition of IPTG at a final concentration of 0.5 mM and allowed to proceed for 5 h. Cells were harvested and lysed by sonication in 50 mM Tris, pH = 8.0, 400 mM NaCl, 1.5 mM TCEP and 1 mM PMSF. The fusion protein was purified over Ni-Sepharose and digested with TEV overnight. C-Cdc37 was separated by a second Ni-Sepharose and subsequently run through a size-exclusion column (Superdex 75) in 50 mM Tris, pH = 8.0, 150 mM NaCl, 1.5 mM TCEP. Prior to NMR studies the protein was further purified through an anion exchange column (HiTrapQ-HP) and buffer exchanged to 50 mM Hepes, pH = 7.5, 100 mM NaCl and 2 mM DTT. Sample concentration ranged between 0.3 and 0.5 mM.

NMR spectroscopy

NMR experiments were carried out at 30 °C on Varian 600 and 800 MHz NMR spectrometers equipped with 5 mm triple resonance cryoprobes. Sequence specific assignment of backbone resonances was performed with information from a set of standard three-dimensional triple resonance spectra, including HNCA, HN(CO)CA, HNCACB, CBCA(CO)NH and HNCO. Side chain resonance assignment was

performed using sequential information from the three-dimensional H(CC)(CO)NH, (H)CC(CO)NH spectra. 94 % of backbone ^{1}H, ^{15}N and ^{13}C (Fig. 1b) and 91 % of sidechain resonances of the C-Cdc37 domain have been assigned and the assignment data have been deposited in the BioMagResBank under the accession number 25740. ^{1}H chemical shifts were referenced to 0 ppm methyl resonance of 2,2-dimthyl-2-silapentane-5-sulfonate (DSS). ^{1}H–^{15}N residual dipolar couplings (RDCs) were measured in the presence of two different pf1 concentrations (15 and 20 mg/ml) using the IPAP ^{1}H–^{15}N HSQC pulse sequence (Ottiger et al. 1998) at 25 °C. High frequency motions (ps–ns timescale) were characterized by measuring {^{1}H}–^{15}N heteronuclear NOEs (Kay et al. 1989), at 800 MHz, in the presence or absence of a 3 s presaturation period prior to the ^{15}N excitation pulse and using recycle delays of 2 and 5 s, respectively. The data with and without NOE were acquired in an fid-interleaved fashion. ^{15}N-R_1 and ^{15}N-R_2 relaxation rates were measured at 800 MHz, using standard pulse sequences (Farrow et al. 1994) without a temperature compensation block, and a recycle delay of 3 s. For R_1 measurements, the delay periods in the series were set to 20 (2×), 50, 100 (2×), 400, 600, 800, 1000, 1200, 1500 and 2000 ms, and for R_2 measurements to 10 (2×), 30 (2×), 50, 70, 90, 110, 210 and 330 ms. The probe temperature was calibrated using MeOH as a standard. To determine the relaxation rate constants, peak heights were fitted to a mono-exponential function in relax (d'Auvergne and Gooley 2008a, b) and errors in peak intensities were taken into account by recording duplicates of two experiments for each of the series. Insights into the motion of the N–H vectors was obtained by the reduced spectral density mapping approach, using scripts in relax. The NMRpipe software package (Delaglio et al. 1995) was used to process all spectra and SPARKY (T. D. Goddard and D. G. Kneller, SPARKY 3, University of California, San Francisco, CS, USA) was used for their analysis.

Structure calculations

The solution structure of C-Cdc37 was solved using conventional NMR approaches, consistent with the small size of the domain. NOE distance restraints were extracted from three dimensional ^{15}N-edited NOESY-HSQC (100 ms), ^{13}C-edited NOESY-HSQC (aliphatic, 100 ms) and ^{13}C-edited NOESY-HSQC (aromatic, 100 ms) spectra. Structure calculations were performed using CYANA 3.97 (Guntert 2004), which combines in an iterative manner automated assignment of NOE cross-peaks with structure calculations. Input for CYANA consisted of all available chemical shift assignments together with the NOESY peak lists from the three three-dimensional edited NOESY spectra. A large number of unambiguously (manually) assigned crosspeaks were included in the original lists and the final run was made using a total of 943 NOE distance restraints (517 short, 243 medium and 183 long) (Table 1). In addition, phi(ϕ) and psi(ψ) torsion angle restraints for protein backbone were predicted using C_a, C_β, H_α, C' and ^{H}N chemical shifts as input to the neural network program *TALOS-N* (Shen and Bax 2013). Only 90 of the torsion angles were predicted as "good" and were included in the calculations (Table 1). 44 hydrogen bond restraints were introduced as a pair of distance restraints (both upper and lower limits) for selected segments of the domain if the following three criteria were simultaneously satisfied: (a) analysis of NOESY spectra revealed a characteristic NOE pattern for regular secondary structure, (b) regular secondary structure elements were predicted for these segments based on backbone chemical shifts and, (c) analysis of {^{1}H}–^{15}N NOEs indicates rigid backbone. The assigned peak lists from the iterative runs of CYANA were manually inspected and incorporated together with 58 RDCs for a final run. A total of 100 were calculated and an ensemble comprised of 10 structures with the lowest energy was analyzed and deposited to the RCSB Protein Data Bank (PDB ID: 2N5X). The structural statistics show a pairwise root mean square deviation (RMSD) of 0.16 Å for the backbone atoms and 0.69 Å for the heavy atoms of the structured region, which includes residues G288-Val343. Structure quality within the ensemble was assessed with PROCHECK (Table 1). In terms of residue geometry

Table 1 NMR structure calculation and statistics for C-Cdc37

NMR constraints	C-Cdc37
Distance constraints	
Total NOE	943
Short range ($\|i-j\| \leq 1$)	517
Medium-range ($1 < \|i-j\| < 5$)	243
Long-range ($\|i-j\| > 5$)	183
Hydrogen bonds	44
Total dihedral angle restraints	
ϕ	45
ψ	45
Residual dipolar couplings	
N–H^{N}	58
Structure statistics	
Average pairwise rms deviation[a] (Å)	
Backbone	0.16
Heavy	0.69
Ramachandran plot statistics[a]	
Residues in most favorable regions (%)	93.6
Residues in additional favorable regions (%)	4.3
Residues in generously favorable regions (%)	2.1
Residues in disallowed regions (%)	0

[a] Refers to the region G288-V343

93.6 % of residues are in the most favored region, 4.3 % in the additionally allowed region, and 2.1 % in the generously allowed region and 0 % in the disallowed regions.

Results and discussion

Solution structure and dynamics of C-Cdc37

The ^{1}H–^{15}N HSQC spectrum of C-Cdc37 (Fig. 1b) is of excellent quality in terms of signal dispersion indicating that the domain boundaries chosen based on the crystal structure of MC-Cdc37 result in a well folded isolated C-Cdc37 domain. Nevertheless no signals can be observed for the region 345–348, either because of conformational exchange broadening or because of rapid chemical exchange with the solvent. Prediction of secondary structure based on backbone chemical shifts performed using the neural network program *TALOS-N*, reveals that C-Cdc37 contains four regions of regular, helical secondary structure (Fig. 1c): 294–300 (α1), 303–311 (α2), 314–322 (α3) and 326–338 (α4). Compared to the available crystal structure (Fig. 1c) the segment 309–315 for which no interpretable electron density is observed forms a short helix, while the extreme C-terminal end of the protein (339–378) is predicted unstructured in solution. In addition, the helical segments α_3 and α_4 are longer by four and two residues, respectively.

These data are in excellent agreement with the dynamic properties of backbone atoms at different timescales. As shown in Fig. 2, all residues between G290 and V343 exhibit $\{^{1}H\}$–^{15}N NOE values greater than 0.7 (average = 0.83), suggesting that the segment encompassing helices α_1–α_4 has a rigid backbone with internal dynamics faster than the overall domain tumbling being absent. On the other hand, residues in the segment 345–378 exhibit low (<0.3) or even negative values suggesting that this is an inherently flexible region, where ps–ns dynamics are operative and ample backbone conformational heterogeneity is present. When backbone ^{15}N relaxation properties are considered, the values of longitudinal relaxation rates, R_1, do not show significant variation and range between 1.5 and 1.9 s^{-1}. Transverse relaxation rates, R_2, on the other hand show significant differences for the two ends of the domain. For the 288–343 segment which includes the predicted structured region α_1–α_4 (294–338) transverse relaxation rates have a mean value of 9.9 s^{-1}. In contrast, for the 35 C-terminal residues that are predicted disordered and have low $\{^{1}H\}$–^{15}N NOEs, this drops to 2.9 s^{-1}. The reduced spectral density functions obtained from R_1, R_2 and $\{^{1}H\}$–^{15}N NOEs, provide information about the conformational properties of C-Cdc37. J(0) is sensitive to ps–ns motions, while the high frequency spectral density $J(0.87\omega_H)$ is sensitive to fast internal motions on a ps timescale. In addition, anomalously large values of the apparent J(0) reflect slow timescale motions (μs–ms), such as conformational exchange processes at specific protein sites, especially when these sites do not exhibit distinct $J(0.87\omega_H)$ or $J(\omega_N)$ spectral densities (Eliezer et al. 2000; Lefevre et al. 1996; O'Sullivan et al. 2009; Wen et al. 2010). Residues in the N-terminal end of the domain (288–343) exhibit high J(0) and low $J(0.87\omega_H)$ values, while the opposite trend is observed for residues in the C-terminal end of the domain (349–378), where low J(0) and high $J(0.87\omega_H)$ values are observed. These data suggest that C-Cdc37 possesses differential dynamic properties and indicate the absence of internal flexibility for the α_1–α_4 segment and the presence of significant internal mobility for the last 30 residues. Notably, J(0) values for the structured region are not uniform. Ten residues including, E299, E303, L305, K307, V314, D329, S339, W342 and V343 have J(0) > 3 ns/rad, and V311 in particular exhibits an unusually large J(0) (9.2 ns rad^{-1}). Thus, helix α_2 and the α_2–α_3 loop, that encompass the crystallographically unstructured (301–308) and crystallographically unresolved (309–315) regions, may participate in slow segmental motions at a μs–ms timescale.

The final ensemble of C-Cdc37 structures analyzed is shown in Fig. 3 and Supplementary Fig. 2, and is comprised of the 10 structures with the lowest energy. The structured region consists of a compact globular bundle of four helices arranged as two pairs of V-shaped hairpins, formed by helices α_1–α_2 and α_3–α_4, packed in a parallel mode against each other. It is noted that besides the 40 N-terminal residues of Cdc37 which are largely invariant, the structured core of C-Cdc37 is the next most conserved region of the cochaperone in higher eukaryotes (Fig. 1d). The solvent exposed faces of the two hairpins, as well as the exposed interface, are lined to a large extend by hydrophobic residues and form a distinct patch on the surface of the protein (Supplementary Fig. 3). In comparison to the X-ray structure, the solution structure of C-Cdc37 shows a similar arrangement for the crystallographically resolved helices α_1, α_3 and α_4 (a.a. 294–300, 317–321 and 328–338), however a relatively high RMSD of 2.15 Å is observed (Fig. 3c). This is attributed to the translocation of the helical registry for helix α_3 toward the carboxy terminus by half a turn (Fig. 3d), which results in the partial burial of hydrophobic sidechains (L317 and I321) and partial exposure of polar residues (D319 and S322) in the solution structure with respect to the crystal structure. The quality of the NMR structure was further validated by measuring RDCs in the presence of 15 or 20 mg/ml Pf1. Overall, a significant reduction is observed for the Q values and a better correlation of predicted and measured RDCs is obtained when the NMR structure is

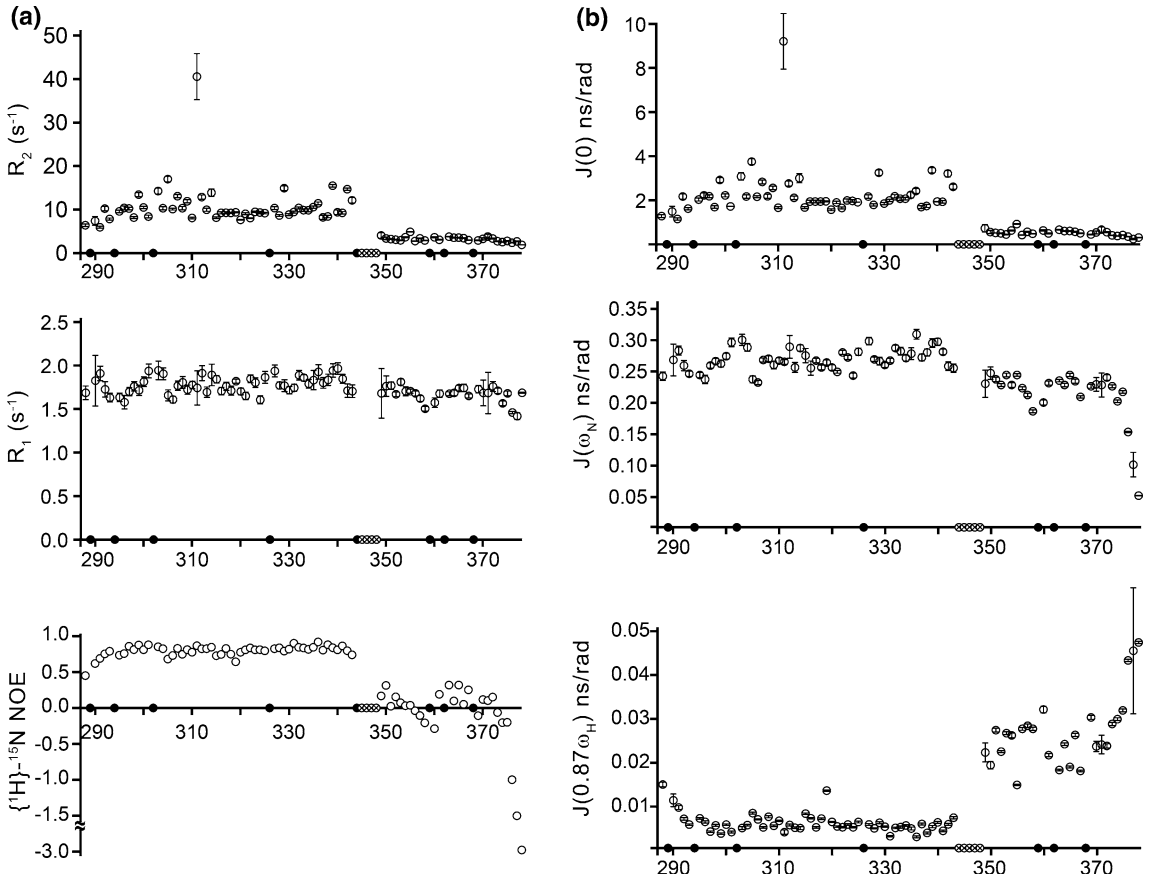

Fig. 2 ^{15}N relaxation data and backbone dynamics of C-Cdc37 recorded at 30 °C as function of residue number. **a** ^{15}N transverse relaxation rate constant, R_2 (*top*), ^{15}N longitudinal relaxation rate constants, R_1 (*middle*) and {^{1}H}–^{15}N heteronuclear NOEs (*bottom*). **b** Reduced spectral density functions of C-Cdc37J(0) (*top*), J(ω_N) (*middle*) and J(0.87ω_H) (*bottom*) determined from the ^{15}N relaxation data shown in (**a**). *Filled circles* on the x-axis denote positions of *prolines* and *circles* with an x-symbol denote unassigned residues

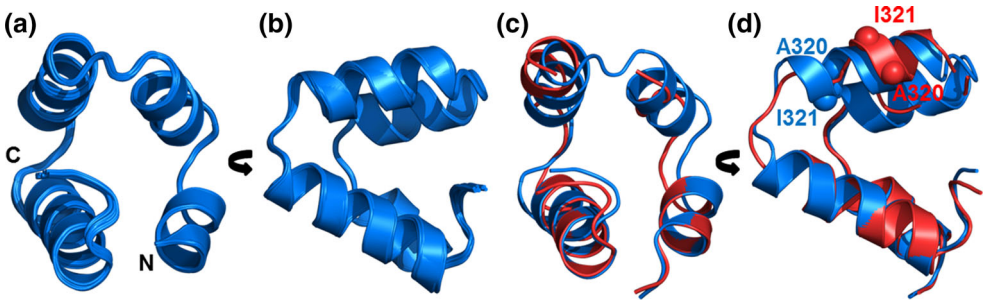

Fig. 3 **a** Overlay of the 10 lowest energy structures of C-Cdc37 aligned over the structured region (a.a. 288–343). The flexible C-terminal segment (a.a. 344–378) is omitted for clarity and the N- and C-terminal ends are denoted as N and C, respectively. **b** Same as (**a**) but rotated by 90°. **c** Overlay of the structure of C-Cdc37 determined in this study by solution NMR (*blue*) and by x-ray crystallography (*red*). No interpretable electron density is observed for the region 309–315, while helix α_2 in the NMR structure appears disordered in the crystal. **d** Same as (**c**) but highlighting Cα atoms of residues A320 and I321 from helix α_3, which shows a shift in the helical registry with respect to the crystal structure

used to predict RDCs at both Pf1 concentrations (Supplementary Fig. 4). A structural comparison within the PDB archive using the PDBeFold server (http://www.ebi.ac.uk/msd-srv/ssm/) does not yield high similarity to any known protein fold. This is also the case for M-Cdc37 and implies that the structure of Cdc37 domains play critical functional roles that are tailored to the chaperoning of protein kinases. Nevertheless, the overall arrangement of the helices is similar to that observed for the PAH domain of Sin 3 (PDB IDs: 2CZY and 2RMR) and for the N-terminal domain of

harmonin (PDB IDs: 2KBQ and 2KBR). Notably, these two domains utilize analogous mechanisms to interact with short stretches of hydrophobic peptides through an exposed hydrophobic surface that possesses similar topology to that identified on C-Cdc37.

Conclusions

The structure of C-Cdc37 was previously determined using X-ray crystallography, in the context of a two-domain fragment, in which the middle domain of the protein was also included (PDB ID: 1US7) (Supplementary Fig. 1) (Roe et al. 2004). As shown in Fig. 3, the solution structure presented in here differs from the crystal structure in the registry of helix α_3 as well as in the conformation of the segment between residues 302 and 316. This segment includes a crystallographically unresolved stretch of seven residues as well as an unstructured segment that adopts a helical conformation in solution. In combination with ^{15}N relaxation measurements, our NMR studies show that a core of fifty highly conserved residues of C-Cdc37 forms a small 4-helical bundle domain, which is connected to a highly flexible 35 residue-long C-terminal tail.

C-Cdc37 has been implicated in the processing of protein kinases by the Hsp90 machinery, but the exact molecular mechanism by which it functions still remains unknown. Substitution of W342 for cysteine causes a lethal defect in drosophila (Cutforth and Rubin 1994), while phosphorylation of Y298 by YES kinase significantly compromises the interaction of the cochaperone with kinase substrates (Xu et al. 2012). The high-resolution NMR structure of C-Cdc37 reported here is essential to understand the interaction of the cochaperone with protein kinases and may serve as a template for the rational design of small molecules that specifically target this region of the protein.

Acknowledgments We thank Prof. Avrom J. Caplan for providing the template plasmid for human Cdc37, Prof. Ralf Landgraf for discussions, Devon Marshal for assisting in manuscript preparation, and USF's *Florida Center of Excellence for Drug Discovery and Innovation* (CDDI) for providing access to the NMR facility. This work was supported in part by an Institutional Research Grant from the American Cancer Society (93-032-16) and by internal funds of the University of South Florida.

References

Bagatell R, Paine-Murrieta GD, Taylor CW, Pulcini EJ, Akinaga S, Benjamin IJ, Whitesell L (2000) Induction of a heat shock factor 1-dependent stress response alters the cytotoxic activity of hsp90-binding agents. Clin Cancer Res 6:3312–3318

Calderwood SK, Khaleque MA, Sawyer DB, Ciocca DR (2006) Heat shock proteins in cancer: chaperones of tumorigenesis. Trends Biochem Sci 31:164–172. doi:10.1016/j.tibs.2006.01.006

Caplan AJ, Mandal AK, Theodoraki MA (2007) Molecular chaperones and protein kinase quality control trends. Cell Biol 17:87–92. doi:10.1016/j.tcb.2006.12.002

Cutforth T, Rubin GM (1994) Mutations in Hsp83 and cdc37 impair signaling by the sevenless receptor tyrosine kinase in Drosophila. Cell 77:1027–1036

d'Auvergne EJ, Gooley PR (2008a) Optimisation of NMR dynamic models I. Minimisation algorithms and their performance within the model-free and Brownian rotational diffusion spaces. J Biomol NMR 40:107–119. doi:10.1007/s10858-007-9214-2

d'Auvergne EJ, Gooley PR (2008b) Optimisation of NMR dynamic models II. A new methodology for the dual optimisation of the model-free parameters and the Brownian rotational diffusion tensor. J Biomol NMR 40:121–133. doi:10.1007/s10858-007-9213-3

Delaglio F, Grzesiek S, Vuister GW, Zhu G, Pfeifer J, Bax A (1995) NMRPipe: a multidimensional spectral processing system based on UNIX pipes. J Biomol NMR 6:277–293

Eliezer D, Chung J, Dyson HJ, Wright PE (2000) Native and non-native secondary structure and dynamics in the pH 4 intermediate of apomyoglobin. Biochemistry 39:2894–2901

Farrow NA et al (1994) Backbone dynamics of a free and phosphopeptide-complexed Src homology 2 domain studied by ^{15}N NMR relaxation. Biochemistry 33:5984–6003

Guntert P (2004) Automated NMR structure calculation with CYANA. Methods Mol Biol 278:353–378. doi:10.1385/1-59259-809-9:353

Jhaveri K, Taldone T, Modi S, Chiosis G (2012) Advances in the clinical development of heat shock protein 90 (Hsp90) inhibitors in cancers. Biochim Biophys Acta 1823:742–755. doi:10.1016/j.bbamcr.2011.10.008

Karnitz LM, Felts SJ (2007) Cdc37 regulation of the kinome: when to hold'em and when to fold'em. Sci Signal 2007:pe22. doi:10.1126/stke.3852007pe22

Kay LE, Torchia DA, Bax A (1989) Backbone dynamics of proteins as studied by ^{15}N inverse detected heteronuclear NMR spectroscopy: application to staphylococcal nuclease. Biochemistry 28:8972–8979

Lefevre JF, Dayie KT, Peng JW, Wagner G (1996) Internal mobility in the partially folded DNA binding and dimerization domains of GAL4: NMR analysis of the N-H spectral density functions. Biochemistry 35:2674–2686. doi:10.1021/bi9526802

McCollum AK, Teneyck CJ, Sauer BM, Toft DO, Erlichman C (2006) Up-regulation of heat shock protein 27 induces resistance to 17-allylamino-demethoxygeldanamycin through a glutathione-mediated mechanism. Cancer Res 66:10967–10975. doi:10.1158/0008-5472.CAN-06-1629

O'Sullivan DB, Jones CE, Abdelraheim SR, Brazier MW, Toms H, Brown DR, Viles JH (2009) Dynamics of a truncated prion protein, PrP(113-231), from (15)N NMR relaxation: order parameters calculated and slow conformational fluctuations localized to a distinct region. Protein Sci 18:410–423. doi:10.1002/pro.44

Ottiger M, Delaglio F, Bax A (1998) Measurement of J and dipolar couplings from simplified two-dimensional NMR spectra. J Magn Reson 131:373–378. doi:10.1006/jmre.1998.1361

Pearl LH (2005) Hsp90 and Cdc37—a chaperone cancer conspiracy. Curr Opin Genet Dev 15:55–61. doi:10.1016/j.gde.2004.12.011

Pearl LH, Prodromou C (2006) Structure and mechanism of the Hsp90 molecular chaperone machinery. Annu Rev Biochem 75:271–294. doi:10.1146/annurev.biochem.75.103004.142738

Polier S, Samant RS, Clarke PA, Workman P, Prodromou C, Pearl LH (2013) ATP-competitive inhibitors block protein kinase recruitment to the Hsp90-Cdc37 system. Nat Chem Biol 9:307–312. doi:10.1038/nchembio.1212

Roe SM, Prodromou C, O'Brien R, Ladbury JE, Piper PW, Pearl LH (1999) Structural basis for inhibition of the Hsp90 molecular chaperone by the antitumor antibiotics radicicol and geldanamycin. J Med Chem 42:260–266. doi:10.1021/jm980403y

Roe SM et al (2004) The mechanism of Hsp90 regulation by the protein kinase-specific cochaperone p50(cdc37). Cell 116:87–98

Rohl A, Rohrberg J, Buchner J (2013) The chaperone Hsp90: changing partners for demanding clients. Trends Biochem Sci 38:253–262. doi:10.1016/j.tibs.2013.02.003

Schwarze SR, Fu VX, Jarrard DF (2003) Cdc37 enhances proliferation and is necessary for normal human prostate epithelial cell survival. Cancer Res 63:4614–4619

Seiler CY et al (2014) DNASU plasmid and PSI: biology-materials repositories— resources to accelerate biological research. Nucleic Acids Res 42:D1253–D1260. doi:10.1093/nar/gkt1060

Shao J, Irwin A, Hartson SD, Matts RL (2003a) Functional dissection of cdc37: characterization of domain structure and amino acid residues critical for protein kinase binding. Biochemistry 42:12577–12588. doi:10.1021/bi035138j

Shao J, Prince T, Hartson SD, Matts RL (2003b) Phosphorylation of serine 13 is required for the proper function of the Hsp90 co-chaperone, Cdc37. J Biol Chem 278:38117–38120. doi:10.1074/jbc.C300330200

Shen Y, Bax A (2013) Protein backbone and sidechain torsion angles predicted from NMR chemical shifts using artificial neural networks. J Biomol NMR 56:227–241. doi:10.1007/s10858-013-9741-y

Sreeramulu S, Gande SL, Gobel M, Schwalbe H (2009a) Molecular mechanism of inhibition of the human protein complex Hsp90-Cdc37, a kinome chaperone-cochaperone, by triterpene celastrol. Angew Chem Int Ed Engl 48:5853–5855. doi:10.1002/anie.200900929

Sreeramulu S, Jonker HR, Langer T, Richter C, Lancaster CR, Schwalbe H (2009b) The human Cdc37.Hsp90 complex studied by heteronuclear NMR spectroscopy. J Biol Chem 284:3885–3896. doi:10.1074/jbc.M806715200

Stepanova L, Finegold M, DeMayo F, Schmidt EV, Harper JW (2000a) The oncoprotein kinase chaperone CDC37 functions as an oncogene in mice and collaborates with both c-myc and cyclin D1 in transformation of multiple tissues. Mol Cell Biol 20:4462–4473

Stepanova L, Yang G, DeMayo F, Wheeler TM, Finegold M, Thompson TC, Harper JW (2000b) Induction of human Cdc37 in prostate cancer correlates with the ability of targeted Cdc37 expression to promote prostatic hyperplasia. Oncogene 19:2186–2193. doi:10.1038/sj.onc.1203561

Vaughan CK et al (2006) Structure of an Hsp90-Cdc37-Cdk4 complex. Mol Cell 23:697–707. doi:10.1016/j.molcel.2006.07.016

Wen Y et al (2010) Unique structural characteristics of the rabbit prion protein. J Biol Chem 285:31682–31693. doi:10.1074/jbc.M110.118844

Whitesell L, Lindquist SL (2005) HSP90 and the chaperoning of cancer. Nat Rev Cancer 5:761–772. doi:10.1038/nrc1716

Xu W et al (2012) Dynamic tyrosine phosphorylation modulates cycling of the HSP90-P50(CDC37)-AHA1 chaperone machine. Mol Cell 47:434–443. doi:10.1016/j.molcel.2012.05.015